Differentiable Reverse-Time Migration for Sound Speed Estimation and Aberration Correction in Medical Pulse-Echo Ultrasound

Rehman Ali*, Trevor Mitcham*, and Nebojsa Duric*

*Department of Imaging Sciences, URMC, Rochester, NY, 14620 USA

ABSTRACT

Sound speed heterogeneities can create aberrations in B-mode ultrasound images by inducing tissue-dependent delays and diffractive effects that conventional beamforming does not incorporate. By using the Fourier split-step method to simulate pressure fields in heterogenous sound speed media, reverse-time migration (RTM) can reconstruct the B-mode image by cross-correlating transmitted and received pressure fields. As a result, RTM is differentiable with respect to sound speed. This enables the reconstruction of the sound speed profile that minimizes the aberration in the B-mode image. In seismic imaging, this form of diffraction tomography, known as wave-equation migration velocity analysis (WEMVA), can roughly be understood as a type of full-waveform inversion (FWI) that acts in the image space (i.e., migrated waveforms) rather than the data space (i.e., traces in the received channel data). This is the first work applying WEMVA to medical pulse-echo ultrasound imaging. Phantom experiments show dramatic improvements in image quality and an 80-87% improvement in point target resolution because of the proposed sound speed estimation and aberration correction scheme.

Keywords: Sound speed estimation, reverse-time migration, diffraction tomography, wave-equation migration velocity analysis

1. INTRODUCTION

An accurate and spatially-resolved sound speed estimate of the tissue can be used to correct aberration in medical pulse-echo ultrasound images. Most sound speed estimators[1–4] rely on an approximate linear relationship between the spatial distribution of slowness (reciprocal of sound speed) in the tissue and aberration delays (or phases) between partial images at each pixel location. A path-length matrix encodes the line-integrals over the slowness distribution corresponding to each aberration delay measurement and is used to reconstruct the sound speed map using regularized inversion. Recent work on differentiable beamforming[5,6] makes the nonlinearity of sound speed estimation more explicit. Typically, the estimation of the aberration delay is done separately from the regularized inversion of the path-length matrix. However, in a differentiable beamforming setup, there is no separate measurement of the aberration delays. Instead, an objective function is defined using the differences between the partial images. The gradient of this objective function directly backprojects errors between these partial images along the corresponding ray paths, and a gradient-descent algorithm is used to converge to the final sound speed estimate, while minimizing aberrations in the image.

Often neglecting both refraction and diffraction, the existing methods for sound speed estimation and distributed aberration correction in B-mode ultrasound rely on ray-based models of the time of flight used in a delay-and-sum beamformer.[2,3,5,6] While reverse-time migration (RTM) has been used to correct aberrations in the B-mode image,[4] the sound speed estimate used in the RTM was the result of ray tomography applied to time shifts measured in the image, representing two distinct processes with inconsistent physical assumptions—the ray tomography used to reconstruct sound speed neglects refraction and diffraction while the RTM used to correct the aberration accounts for both. By directly differentiating RTM with respect to sound speed, both sound speed estimation and aberration correction becomes unified under a single consistent framework that fully accounts for refraction and diffraction. In seismic imaging, this framework came to be known as wave-equation migration velocity analysis (WEMVA).[7,8] The purpose of this work is to demonstrate the application of WEMVA to medical pulse-echo ultrasound imaging.

Further author information: (Send correspondence to Rehman Ali)
Rehman Ali: E-mail: Rehman$_{A}li@URMC.Rochester.edu$

Medical Imaging 2026: Ultrasonic Imaging and Tomography, edited by Christian Boehm, Mohammad Mehrmohammadi, Shawn Liangzhong Xiang, Proc. of SPIE Vol. 13931, 1393103 · 2026 Published by SPIE
1605-7422 · doi: 10.1117/12.3085607

2. BACKGROUND

2.1 Fourier Split-Step Angular Spectrum Method

Ultrasonic wave-fields $p(x, z, f)$ as a function of location (x, z) and frequency f can be propagated from a depth of z to $z + \Delta z$ using the Fourier split-step method:[4, 9–11]

$$p(x, z + \Delta z, f) = W(x) S_{\pm}(x, z, f) \mathcal{F}^{-1}_{k_x \mapsto x} H_{\pm}(k_x, z, f) \mathcal{F}_{x \mapsto k_x} p(x, z, f), \tag{1}$$

$$H_{\pm}(k_x, z, f) = \exp\left(\pm j 2\pi \left((f\bar{s}(z))^2 - k_x^2\right)^{1/2} \Delta z\right), \tag{2}$$

$$S_{\pm}(x, z, f) = \exp\left(\pm j 2\pi f s_{res}(x, z) \Delta z\right), \tag{3}$$

$$\bar{s}(z) = \frac{1}{L} \int_{-L/2}^{L/2} s(x, z) dx, \tag{4}$$

$$s_{res}(x, z) = s(x, z) - \bar{s}(z). \tag{5}$$

where $\mathcal{F}_{x \mapsto k_x}$ and $\mathcal{F}^{-1}_{k_x \mapsto x}$ are the forward and inverse Fourier transforms in the lateral dimension (x), $W(x)$ is an anti-aliasing window used to suppress wrap-around in the lateral dimension, $s(x, z)$ is the slowness (i.e., reciprocal of sound speed) in the medium as a function of (x, z), and L is the lateral length of the computational domain over which the angular spectrum method is applied.

Because this is a Fourier split-step scheme, we decompose $s(x, z)$ into an axially-varying component $\bar{s}(z)$ and a laterally varying component $s_{res}(x, z)$: $H_{\pm}$ is bulk propagation via the angular spectrum method at a slowness $\bar{s}(z)$, and $S_{\pm}$ is a phase screen correction involving the laterally-varying component $s_{res}(x, z)$.

2.2 Frequency-Domain Implementation of Reverse-Time Migration (RTM)

Pulse-echo ultrasound images can be created by propagating transmit and receive wavefields $p_{tx(i)}(x, z, f)$ and $p_{rx(i)}(x, z, f)$ based on the receive channel data collected from pulses emitted by each transmit element $i = 1, ..., N$. Partial images $I_i(x, z)$ can be formed prior to amplitude detection based on the following equations:

$$I_i(x, z) = \int_0^{\infty} p^*_{tx(i)}(x, z, f) p_{rx(i)}(x, z, f) df, \tag{6}$$

$$p_{tx(i)}(x, z + \Delta z, f) = W(x) S_{-}(x, z, f) \mathcal{F}^{-1}_{k_x \mapsto x} H_{-}(k_x, z, f) \mathcal{F}_{x \mapsto k_x} p_{tx(i)}(x, z, f), \tag{7}$$

$$p_{rx(i)}(x, z + \Delta z, f) = W(x) S_{+}(x, z, f) \mathcal{F}^{-1}_{k_x \mapsto x} H_{+}(k_x, z, f) \mathcal{F}_{x \mapsto k_x} p_{rx(i)}(x, z, f), \tag{8}$$

where $\hat{p}_{tx(i)}(k_x, f) = p_{tx(i)}(k_x, z = 0, f)$ and $\hat{p}_{rx(i)}(k_x, f) = p_{rx(i)}(k_x, z = 0, f)$ represent the frequency spectra of the transmit pulse and receive channel data from each element on the array (located at $z = 0$).

Apodization[12] was applied to the receive channel data to maximize the lag-one coherence between images from neighboring transmit elements. Propagation via the Fourier split-step angular spectrum method should correct for aberration by accounting for the true sound speed in the medium. Equations (6)-(8) describe a frequency-domain implementation of reverse-time migration (RTM), which reconstructs each partial image by correlating the corresponding transmitted and received wavefields.

2.3 Wave-Equation Migration Velocity Analysis (WEMVA)

Because each simulated wavefield is a function of the slowness profile $\vec{s}$ [vectorization of $s(x, z)$], the partial images $I_i(x, z; \vec{s})$ produced by RTM are also a function of the slowness profile. Wave-equation migration velocity analysis (WEMVA) directly minimizes the errors (i.e., aberrations) between these partial images via the following nonlinear least-squares objective function:

$$E(\vec{s}) = \frac{1}{2} \sum_{x,z} \sum_{i=1}^{N_{tx}-1} \left| I_{i+1}(x, z; \vec{s}) - I_i(x, z; \vec{s}) \right|^2. \tag{9}$$

To simplify gradient evaluation, automatic differentiation software known as JAX[13] was used to implement equations (1)-(8). Regularization was also used to smooth the gradient image calculated by JAX.[4] This gradient calculation was used inside a conjugate gradient algorithm to minimize (9) with respect to $\vec{s}$. Starting from a spatially constant 1540 m/s sound speed guess, we apply 50 iterations of conjugate gradient with the WEMVA objective function (9) to reconstruct the sound speed profile and correct the aberrations in the image.

2.4 Target-Following Grid: Adaptive Depth Spacing for the Angular Spectrum Method

On a fixed uniform image grid, image points are placed uniformly in depth according to $z_k = z_0 + k\Delta z$. However, as we change $\vec{s}$, an image target initially placed at a depth z_k may appear deeper or shallower. Ideally, the value of z_k would change with $\vec{s}$ such that it always corresponds to the same image target.[14] This adaptive depth grid would be equally spaced in time rather than depth according to $z_k = z_0 + \sum_{n=1}^{k} c_n \Delta t$, where c_n is the reciprocal-average sound speed in layer n. In other words, rather than maintain a constant depth-spacing Δz, we instead calculate a variable $\Delta z = \bar{c}(z)\Delta t$ that maintains a constant time-spacing $\Delta t = \bar{s}(z)\Delta z$ (where $\bar{c}(z) = 1/\bar{s}(z)$).

3. METHODS

3.1 Imaging Studies: Simulation and Experiment

All imaging in this study was performed using a Verasonics Vantage 256 ultrasound system (Verasonics Inc., Kirkland, WA, USA) with an 8 MHz center-frequency L12-5 50mm transducer (Advanced Technology Laboratories, Inc., Bothell, WA, USA). Hadamard pulse sequences were used to maximize the signal-to-noise ratio. Additional imaging studies based on simulation work[4] in k-Wave[15] are also presented.

3.2 Phantom Fabrication

All tissue-mimicking phantoms in this work were fabricated with 8% gelatin (SigmaAldrich, St. Louis, MO, USA), 2.5% silica (US Silica, Katy, TX, USA), 89.4% deionized water, and 0.1% glutaraldehyde (SigmaAldrich). Point targets which consisted of 36-GA (250-μm diameter) wire (McMaster-Carr) were included as imaging targets within all phantoms. To this end, 6/16-inch diameter holes were drilled on opposite sides of a 4-inch acrylic 5-sided cube so that the wires could be inserted in a repeatable manner. Additionally, hypo-echoic lesions consisting of 8% gelatin, 0.5% silica, 91.4% deionized water, and 0.1% glutaraldehyde were included in several phantoms. These inclusions were cast by drilling 6/16-inch diameter holes below the wire inclusions on one side, inserting a closed tube while pouring the gelatin background, and then back-filling the negative space after the tube's removal. Gelatin inclusions with an increased sound speed (¿1600 m/s) were also cast above the wire targets in several phantoms using a similar technique, but using 8% gelatin, 2.5% silica, 69.4% deionized water, 20% isopropanol, and 0.1% glutaraldehyde to fill the negative space.

4. RESULTS AND DISCUSSION

The k-Wave simulations[15] in the prior work[4] were reused here to provide an initial demonstration of sound speed estimation and aberration correction using WEMVA. The k-Wave simulations in Figure 1 show that the full width at half-maximum (FWHM) resolution improves from 2.19 ± 0.92 mm to 0.30 ± 0.02 mm when transitioning from using a constant 1540 m/s sound speed to using WEMVA to iteratively estimate the sound speed profile that best focuses the ultrasound signals. The tissue mimicking phantoms, fabricated using the methods described herein, were used to demonstrate WEMVA in experimental data. The 20% isopropyl alcohol inclusions inside each phantom provided a significant increase in sound speed which caused high levels of aberration in both point targets and hypoechoic targets. Figure 2 shows the sound speed estimate and aberration correction in each phantom based on WEMVA. In the top and bottom phantoms, the improvement in point-target resolution is 80.16 ± 14.97 % and 87.29 ± 11.71 %, respectively.

The same phantoms shown in Figure 2 were used in the prior work[4] to validate the aberration correction based on the sound speed reconstructed by ray tomography. In that earlier work,[4] although the aberration corrections resulting from the ray-based sound speed estimates were a significant improvement upon the 1540 m/s assumption, these corrections were far from perfect. Later work[5] showed that differentiable beamforming, based on minimizing the common midpoint phase error, improved the focusing in the image reconstruction corresponding to the phantom used in the top row of Figure 2, achieving nearly perfect focusing everywhere in the image. This work achieves a similar improvement in focusing everywhere in the image based on WEMVA, without relying on a common midpoint configuration. The present work on WEMVA can be improved further by incorporating either the common midpoint (CMP) strategies[5,16–19] used in multstatic imaging or the common midangle (CMA) strategy used in plane-wave imaging.[2,20] Both CMP and CMA strategies maximize the correlation between backscattered echoes by isolating the two-way transmit-and-receive contributions to aberration.

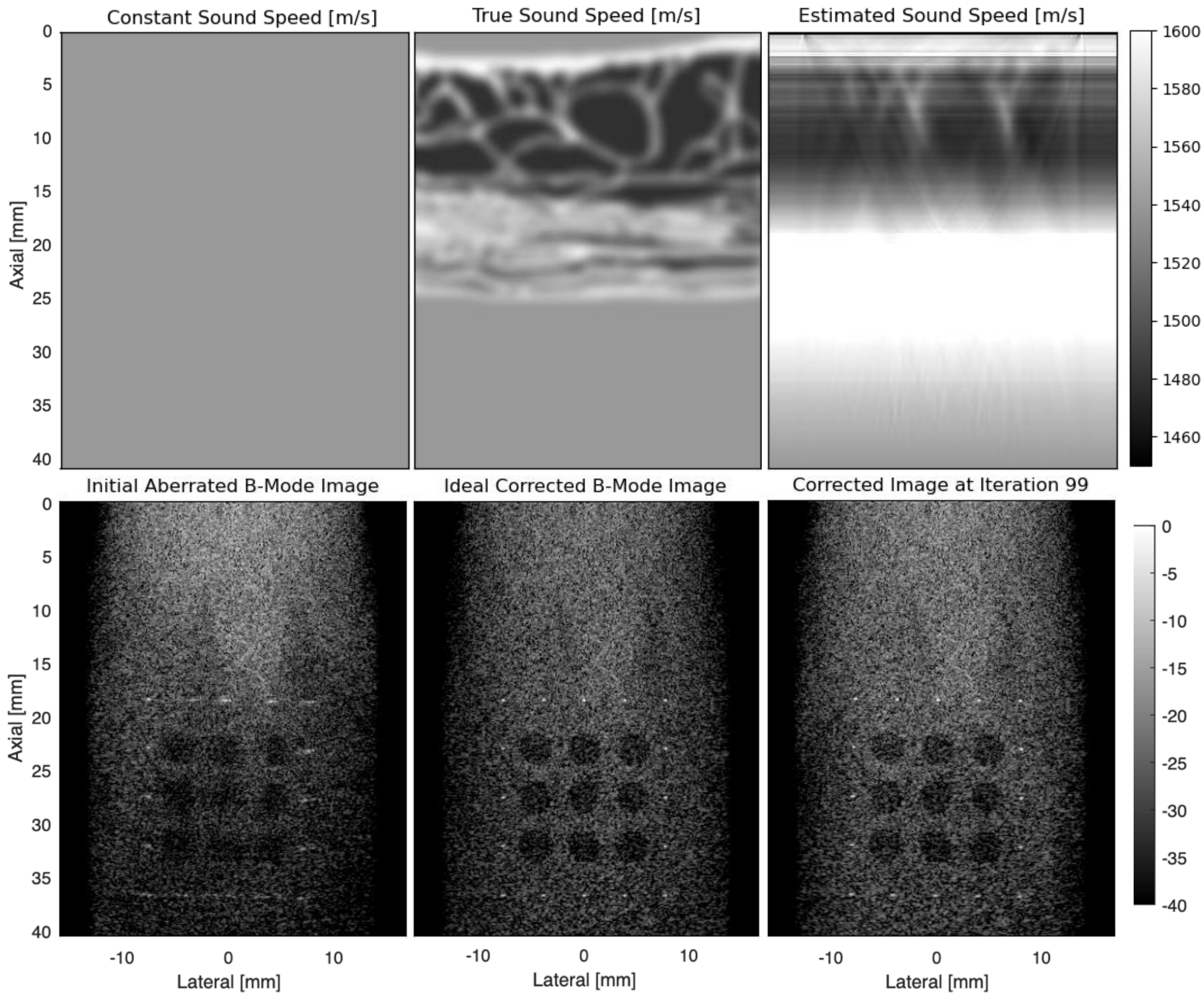

Figure 1. Proof-of-Concept Demonstration of WEMVA for Sound Speed Estimation and Phase Aberration Correction in k-Wave Simulations. When using a homogenous 1540 m/s sound speed to reconstruct the B-mode image, the full width at half maximum (FWHM) resolution of the image targets at 36 mm depth are 2.19 ± 0.92 mm. Using the true sound speed profile yields a FWHM point-target resolution of 0.28 ± 0.02 mm. The WEMVA sound speed estimate results in a FWHM resolution of 0.30 ± 0.02 mm.

The objective function (9) used in this work relies primarily on measuring the one-way aberration caused by different transmit paths to the transducer; however, as discussed in previous work,[6,21] the gradient of the objective function (9) yields nonzero contributions to all the receive paths back to the transducer, even if the dominant contribution to the gradient is from the individual transmit paths to the image point. This work maximizes the lag-one coherence that can be achieved between neighboring transmit elements from a single common receive apodization profile.[12] However, if the receive apodization can vary between transmissions, the CMP-based translating-transmit-aperture (TTA) algorithm,[18,19] can further maximize this correlation to one. On the other hand, the CMA approach[2,20] operates in the k-space of the reflection image by using a filter to isolate specific mid-angles. Therefore, the CMA induces the two-way transmit-and-receive contributions to aberration via a filtering operation in k-space.

Although the CMP approach is specific to a multistatic imaging scenario, the CMA approach can be generalized across a variety of imaging sequences (e.g., plane-wave and virtual-source synthetic aperture). Differentiable

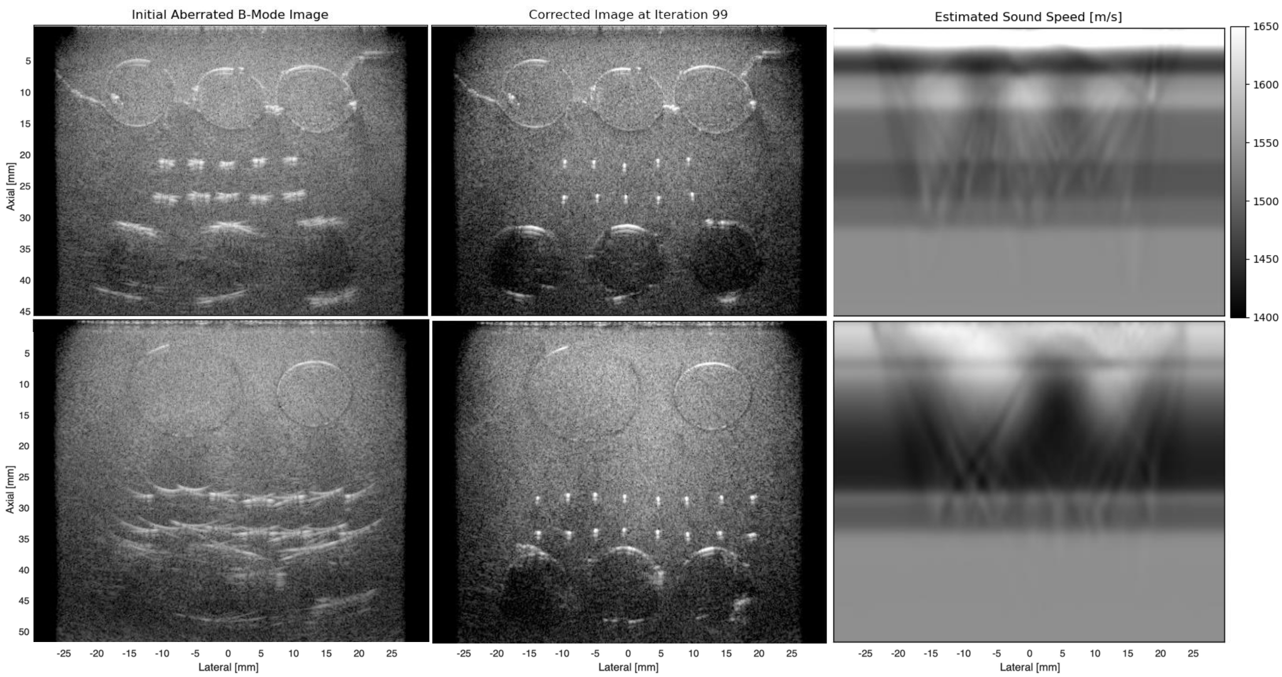

Figure 2. Sound Speed Estimation and Aberration Correction in Phantoms. All B-mode images are shown on an 80 dB dynamic range. In the top phantom, the full width at half maximum (FWHM) decreases from 1.25 ± 0.56 mm to 0.18 ± 0.01 mm, an 80.16 ± 14.97 % improvement in point target resolution. In the bottom phantom, the FWHM resolution decreases from 2.81 ± 1.88 mm to 0.28 ± 0.08 mm, which is an 87.29 ± 11.71 % improvement in point target resolution. In both phantoms, the menisci of the hypoechoic inclusions below the point targets are well focused after applying WEMVA to estimate the sound speed profile and correct the aberrations in the image.

beamforming, currently based on common midpoint phase error, is primarily constrained to multistatic synthetic aperture,[5] which may require recovery of full-matrix capture data from another imaging sequence.[22] Because RTM generalizes to a much wider variety of imaging sequences, WEMVA can be used to reconstruct sound speed and correct aberrations outside of multistatic imaging. As a result, the CMA approach may be more suitable for the generalized use case for WEMVA. In addition, RTM can further incorporate time shift and spatial offset.[23] For example, the spatial-offset extension is conceptually similar to the distortion matrix approach for random-scattering media,[24] and the time-shift extension used in prior work[4] can be used to isolate time delays. These extensions of RTM enable alternative implementations of WEMVA for sound speed estimation and aberration correction in medical pulse-echo ultrasound.

5. CONCLUSIONS

This work demonstrates a differentiable reverse-time migration, also known as wave-equation migration velocity analysis (WEMVA), that reconstructs the sound speed profile by minimizing aberrations in the ultrasound image. This is the first work to apply wave-equation migration velocity analysis (WEMVA) to handheld pulse-echo ultrasound. As a type of image-domain full-waveform inversion, WEMVA iteratively reconstructs the sound speed profile that minimizes phase aberrations in the ultrasound. Relative to prior work on differentiable beamforming, the main advantage of WEMVA is the underlying wave propagation model that accounts for both refraction and diffraction. Phantom experiments show an 80-87% improvement in point target resolution with dramatic improvements in image quality.

ACKNOWLEDGMENTS

This work was supported by the National Institute of Biomedical Imaging and Bioengineering (NIBIB) from the National Institute of Health (NIH) under grants F32-EB034589 and K99-EB037080 (Contact PI: Rehman Ali).

REFERENCES

[1] Podkowa, A. S. and Oelze, M. L., "The convolutional interpretation of registration-based plane wave steered pulse-echo local sound speed estimators," *Physics in Medicine & Biology* **65**(2), 025003 (2020).

[2] Stähli, P., Kuriakose, M., Frenz, M., and Jaeger, M., "Improved forward model for quantitative pulse-echo speed-of-sound imaging," *Ultrasonics* **108**, 106168 (2020).

[3] Schweizer, D., Rau, R., Bezek, C. D., Kubik-Huch, R. A., and Goksel, O., "Robust imaging of speed of sound using virtual source transmission," *IEEE Transactions on Ultrasonics, Ferroelectrics, and Frequency Control* **70**(10), 1308–1318 (2023).

[4] Ali, R., Mitcham, T. M., Singh, M., Doyley, M. M., Bouchard, R. R., Dahl, J. J., and Duric, N., "Sound speed estimation for distributed aberration correction in laterally varying media," *IEEE transactions on computational imaging* **9**, 367–382 (2023).

[5] Simson, W., Zhuang, L., Frey, B. N., Sanabria, S. J., Dahl, J. J., and Hyun, D., "Ultrasound autofocusing: Common midpoint phase error optimization via differentiable beamforming," *IEEE Transactions on Medical Imaging* (2025).

[6] Ali, R., Mitcham, T., Singh, M., Bouchard, R., Doyley, M., Dahl, J., and Duric, N., "Iterative sound speed tomography for distributed aberration correction," in [*2023 IEEE International Ultrasonics Symposium (IUS)*], 1–4, IEEE (2023).

[7] Sava, P. and Biondi, B., "Wave-equation migration velocity analysis. i. theory," *Geophysical Prospecting* **52**(6), 593–606 (2004).

[8] Perrone, F., Sava, P., Andreoletti, C., and Bienati, N., "Linearized wave-equation migration velocity analysis by image warping," *Geophysics* **79**(2), S35–S46 (2014).

[9] Schwab, H.-M. and Schmitz, G., "Full-wave ultrasound reconstruction with linear arrays based on a fourier split-step approach," in [*2018 IEEE International Ultrasonics Symposium (IUS)*], 1–4, IEEE (2018).

[10] Jiang, C., Li, Y., Xu, K., and Ta, D., "Full-matrix phase shift migration method for transcranial ultrasonic imaging," *IEEE transactions on ultrasonics, ferroelectrics, and frequency control* **68**(1), 72–83 (2020).

[11] Vyas, U. and Christensen, D., "Ultrasound beam simulations in inhomogeneous tissue geometries using the hybrid angular spectrum method," *IEEE transactions on ultrasonics, ferroelectrics, and frequency control* **59**(6), 1093–1100 (2012).

[12] Ali, R., Duric, N., and Dahl, J. J., "Optimal transmit apodization for the maximization of lag-one coherence with applications to aberration delay estimation," *Ultrasonics* **132**, 107010 (2023).

[13] Bradbury, J., Frostig, R., Hawkins, P., Johnson, M. J., Leary, C., Maclaurin, D., Necula, G., Paszke, A., VanderPlas, J., Wanderman-Milne, S., et al., "Jax: Autograd and xla," *Astrophysics Source Code Library* , ascl–2111 (2021).

[14] Ahmed, R. and Trahey, G. E., "Spatial ambiguity correction in coherence-based average sound speed estimation," *IEEE transactions on ultrasonics, ferroelectrics, and frequency control* **71**(10), 1244–1254 (2024).

[15] Treeby, B. E. and Cox, B. T., "k-wave: Matlab toolbox for the simulation and reconstruction of photoacoustic wave fields," *Journal of biomedical optics* **15**(2), 021314–021314 (2010).

[16] Haun, M. A., Jones, D. L., and Oz, W., "Overdetermined least-squares aberration estimates using common-midpoint signals," *IEEE transactions on medical imaging* **23**(10), 1205–1220 (2004).

[17] Ali, R., Hyun, D., and Dahl, J. J., "Application of common midpoint gathers to medical pulse-echo ultrasound for optimal coherence and improved sound speed estimation in layered media," in [*2020 IEEE International Ultrasonics Symposium (IUS)*], 1–4, IEEE (2020).

[18] Ng, G., Walker, W., and Trahey, G., "Improvement of signal correlation for adaptive imaging using the translating transmit aperture algorithm," in [*1996 IEEE Ultrasonics Symposium. Proceedings*], **2**, 1395–1400, IEEE (1996).

[19] Ng, G. C., Freiburger, P. D., Walker, W. F., and Trahey, G. E., "A speckle target adaptive imaging technique in the presence of distributed aberrations," *IEEE transactions on ultrasonics, ferroelectrics, and frequency control* **44**(1), 140–151 (2002).

[20] Haun, M. A., Jones, D. L., and O'Brien, W. D., "Aberration correction with off: the overdetermined, fan-filtering algorithm," in [*IEEE Symposium on Ultrasonics, 2003*], **2**, 1231–1234, IEEE (2003).

[21] Ali, R., "Open-source full-waveform ultrasound computed tomography based on the angular spectrum method using linear arrays," in [*Medical Imaging 2022: Ultrasonic Imaging and Tomography*], **12038**, 187–205, SPIE (2022).

[22] Ali, R., Herickhoff, C. D., Hyun, D., Dahl, J. J., and Bottenus, N., "Extending retrospective encoding for robust recovery of the multistatic data set," *IEEE transactions on ultrasonics, ferroelectrics, and frequency control* **67**(5), 943–956 (2019).

[23] Sava, P. and Fomel, S., "Time-shift imaging condition in seismic migration," *Geophysics* **71**(6), S209–S217 (2006).

[24] Lambert, W., Cobus, L. A., Frappart, T., Fink, M., and Aubry, A., "Distortion matrix approach for ultrasound imaging of random scattering media," *Proceedings of the National Academy of Sciences* **117**(26), 14645–14656 (2020).